Intricate mechanism (s) of substrate specificity and loss of function on disease mutation (K211N) of Parkin

Dipti Ranjan Lenka, Shradha Chaurasiya, and Atul Kumar[#]

Department of Biological Sciences, Indian Institute of Science Education and Research (IISER) Bhopal, Bhopal, India, 462066.

[#] Correspondence should be addressed to atul@iiserb.ac.in

Abstract

Parkin mutations lead to the early onset of Parkinson's disease. PINK1-mediated phosphorylation of its substrates Ubiquitin (Ub)-like proteins (NEDD8, Ubiquitin) and Ubiquitin-like (Ubl) domain activate autoinhibited Parkin. Substrate specificity on Parkin and the cause of loss of function in disease mutation K211N remain elusive. Herein, we determine the first crystal structure of human Parkin bound with pNEDD8 and establish the mechanism of substrate specificity on Parkin. RING0 pocket is specific for pUbl and does not bind with pUb/pNEDD8. In contrast, the RING1 pocket is more robust for binding with pNEDD8. Also, the binding of activators in the RING1 and RING0 pockets of Parkin leads to a distinct extent of conformational changes in the RING2 domain. The crystal structure of Parkin K211N reveals intriguing conformational changes that lock RING2 with RING0, thus inhibiting Parkin independent of its binding with pUb/pNEDD8. This study would help design small-molecule Parkin activators against Parkinson's disease.

Introduction

PARK2 and PARK6 genes encode Parkin E3 ligase and PINK1 (PTEN-induced putative kinase 1). Mutations in PARK2 and PARK6 genes cause Parkinson's Disease (PD). Parkin and PINK1 control the mitochondrial homeostasis process autophagy (mitophagy) of the damaged mitochondria [1–7].

Parkin is a member of RBR family E3 ligase consisting of an N-terminal ubiquitin-like (Ubl) domain followed by four Zn2+ binding domains RING0, RING1, inbetweenRING (IBR), and RING2 domains [8–10]. Like other members of the RBR family E3 ligase, Parkin catalytic C431 (on RING2) is charged with ubiquitin in an E2-dependent manner before the transfer of ubiquitin on lysines of its substrate [11–13]. Parkin is an autoinhibited cytosolic

protein [8]. The E2 binding site on Parkin is blocked by the presence of Ubl on RING1. A short repressor (REP) element between IBR and RING2 also restricts E2 binding. RING0, which occludes catalytic C431 on RING2, significantly inhibits Parkin activity [8,10,14,15].

Phosphorylation of S65 on ubiquitin by PINK1 leads to the recruitment of Parkin on mitochondria, mediated by enhanced interaction between RING1 of Parkin and pUb [16–19]. Conserved S65 of the Ubl domain of Parkin is phosphorylated by PINK1 [20,21], leading to fully active Parkin conformation by binding pUbl in the RING0 pocket. RING0 pocket (comprising K161, R163, and K211) and RING1 pocket (comprising R305, H302, and K151) bind with phospho-S65 group of phosphorylated Parkin activators [22–27]. Recently, PINK1-mediated S65 phosphorylation on another ubiquitin-like protein, NEDD8, was shown to activate Parkin [28]. While several crystal structures of Parkin with pUb are known [22,23,26,27,29,30], the structure of pNEDD8 and Parkin complex is not available to reveal its molecular mechanism. Furthermore, it remains unclear whether the two pockets (RING0 and RING1) on Parkin recognize different Parkin activators (pUbl, pUb, and pNEDD8) specifically or promiscuously, as suggested by recent publications [29,31].

Recent publications suggested two pUb binding sites on Parkin, one in the RING1 pocket and another in the RING0 pocket [29,31]. These publications demonstrated that disease mutation K211N showed loss of Parkin activation in the presence of pUb and loss of Parkin localization to the mitochondria [31]. Parkin construct lacking the RING2 domain was used to demonstrate the binding of pUb in both RING0 and RING1 pockets, and K211N led to the loss of pUb binding in the RING0 pocket [29,31]. A new feedforward pathway of Parkin activation was proposed where pUb binding is preferred over pUbl binding in the RING0 pocket [29,31]. Our recent work demonstrated that RING2 negatively affects pUbl binding in the RING0 pocket [30]. The presence of RING2 could provide specificity in the RING0 and needs to be tested. Also, in our recent work, Parkin K211N (C431F), unlike Parkin H302A (C431F), did not show any defect in its translocation to the mitochondria when co-expressed with native Parkin [30]. The latter warrants a detailed biophysical study to understand the loss of Parkin activation in disease mutation K211N.

Herein, we solved the structure of Parkin with pNEDD8, which shows the binding of pNEDD8 in the RING1 pocket where pUb binds. However, the structure shows new interactions between pNEDD8 mediated by favorable residues on NEDD8 that are not conserved on pUbl or pUb. Ubiquitination assays further supported the latter to establish a more robust activation of Parkin by pNEDD8 compared to pUb. We also demonstrate that pNEDD8/pUb specifically binds in the RING1 pocket and does not cross-react with the

RING0 pocket. We demonstrate that specificity in RING0 and RING1 is mediated by unique charge distribution on Parkin surrounding the basic residues that bind phospho-S65 of pUbl or pUb/pNEDD8. Similarly, charge distribution around phospho-S65 of pUbl and pUb/pNEDD8 is more favorable for specific binding in the RING0 and RING1 pockets, respectively. Our data also suggests that unlike binding in the RING0 pocket, which results in large conformational changes in RING2, binding in the RING1 pocket does not show large conformational changes in RING2. Furthermore, we demonstrate that disease mutation K211N on Parkin perturbs E3 ligase activity independent of Parkin activators (pUb/pNEDD8) binding, unlike previously suggested. We solved the structure of K211N Parkin with pNEDD8, which reveals new conformational changes in RING0, leading to new interactions between RING0 and RING2. These new interactions restrict the movement of RING2 in Parkin K211N, leading to the loss of E3 ligase activity independent of pUb binding. Overall, this study would help therapeutic efforts to develop small-molecule activators against Parkin, specifically against mutants such as K211N that lead to extreme defects and were proposed to lack binding with activators.

Results

pNEDD8 leads to more robust activation of Parkin

Recent publications suggested two pUb binding sites on Parkin, one in the RING1 pocket and another in the RING0 pocket where pUbl binds [29,31]. Another study showed NEDD8 phosphorylation by PINK1, leading to Parkin activation [28]. While the phosphorylation of different ubiquitin-like proteins by PINK1 and their binding on Parkin is well known, the selectivity and specificity in the above pathway remain elusive. To test the specificity between pUb and pNEDD8, we performed ubiquitination assays on Parkin using increasing concentrations of pUb and pNEDD8. Interestingly, we noticed that pNEDD8-mediated Parkin activation is significantly higher than pUb-mediated Parkin activation (Fig. 1A). Interestingly, assays performed using unphosphorylated NEDD8 and Ub also show higher activation of Parkin with NEDD8 (Fig. 1B). Overall, our data suggested that NEDD8 is a better activator of Parkin than Ub.

pNEDD8 bound crystal structure confirms robust binding between Parkin and NEDD8

As our activity assays suggest that NEDD8 is a better substrate than Ub (Fig 1), we wanted to understand the molecular details of NEDD8 and Parkin interaction. Unlike pUb and human Parkin structure [22,26,30], we crystallized the complex of pNEDD8 and human Parkin without any chemical modification/artificial tethering. Human R0RBR and pNEDD8 complex was purified over size-exclusion chromatography and crystallized. The structure of R0RBR and

pNEDD8 was determined at 2.25 Å (Extended Data Table 1). The overall structure of the Parkin and pNEDD8 complex was quite similar to the Parkin and pUb complex (Extended Data Fig. 1A). Although RING2 is not displaced (Extended Data Fig. 1B), we noticed a significantly higher B-factor for RING2 in pNEDD8 bound Parkin structure (Fig. 2A). Higher B-factor indicates the flexibility caused in the RING2 region of Parkin due to pNEDD8 binding in the RING1 pocket.

Closer inspection of Parkin structures with pUb or pNEDD8 reveals some minor conformational changes on Helix-1 (H1) of Parkin. For example, Q317 is away from pUb interface in pUb bound Parkin structure (Fig. 2B, 2C), whereas Q317 is present at the interface of pNEDD8 (Fig. 2B, 2D) and forms hydrogen bond with H68 of pNEDD8 (Fig. 2D). Beside the conserved interactions between Parkin and pUb or pNEDD8, new interactions are also seen between Parkin and pNEDD8. For example, S46 of pNEDD8 forms a hydrogen bond with Q316 of Parkin (Fig. 2D). Y45 of pNEDD8 forms hydrogen bonds with Y312 and H302 of Parkin (Fig. 2D). Furthermore, K60 of pNEDD8 forms a hydrogen bond with the carbonyl of L187 of Parkin (Fig. 2D). In addition to the above hydrogen bonds, L62 of pNEDD8 forms hydrophobic interactions with V224 of Parkin. Interestingly, among all known Ubls, which can be phosphorylated by PINK1, the above residues are only present in pNEDD8 and replaced by unfavorable residues in Ubl and Ub (Fig. 2E). These new interactions explain the higher activation by NEDD8 in Figure 1, thus suggesting NEDD8 would be a preferred substrate for binding in the RING1 pocket of Parkin.

Parkin activators (pNEDD8/pUb) specifically bind in the RING1 pocket

Recent publications suggested that the RING0 pocket (comprising K211) binds with pUb and leads to the feedforward loop of Parkin activation [29,31]. These publications used constructs lacking RING2 and showed binding of pUB in RING0 and RING1 pockets. Our recent work demonstrated that RING2 negatively affects the pUbl binding in the RING0 [30]. Therefore, we wondered whether the presence of RING2 would provide specificity to select Parkin activator in the RING0 pocket. To test this, we used untethered (TEV treated) R0RBR (RING0-RING1-IBR-REP-RING2, TEV site between IBR & REP) protein and performed the RING2 displacement assay similar to our recent research, which showed displacement of RING2 from untethered Parkin by pUbl/pParkin in trans [30]. We noticed that both pUb or pNEDD8 form complex with untethered R0RBR (Fig. 3A, Extended Data Fig. 2A). However, pUb/pNEDD8 binding failed to displace RING2 from RING0 as suggested by co-elution of REP-RING2 with R0RB (RING0-RING1-IBR) and pUb/pNEDD8 (Fig. 3A, Extended Data

Fig. 2A), unlike pUbl/pParkin binding in trans that displace REP-RING2 from Parkin core [30]. Interestingly, pNEDD8, which binds and activates Parkin stronger than pUb (Fig. 1), also failed to result in REP-RING2 displacement (Extended Data Fig. 2A). Furthermore, K211N mutation in the RING0 domain did not affect the complex formation between Parkin and pUb/pNEDD8 (Fig. 3B, Extended Data Fig. 2B). However, as expected H302A mutation in the RING1 domain perturbs the complex formation between Parkin and pUb/pNEDD8 (Fig. 3C, Extended Data Fig. 2C). In any of the above conditions, unlike pUbl/pParkin binding in the RING0 pocket displacing the RING2 domain in trans [30], RING2 displacement was not observed suggesting that pUb/pNEDD8 binds specifically in the RING1 pocket. This data also suggests that RING2 domain movement after pUb binding is not as drastic as suggested earlier [29,31]. The latter is consistent with the B-factor analysis of the crystal structure in Fig. 2A, which suggested flexibility, not complete displacement, in the RING2 domain after pNEDD8 binding. Overall, this data suggests the specific nature of two pockets on Parkin and conformational changes to different magnitudes.

Disease mutation K211N perturbs Parkin activity independent of activator (pUb/pNEDD8) binding

Previous data showed that K211N mutation on Parkin leads to loss of pUb-mediated Parkin activation [23,31]. As our data in Figure 3/Extended Data Figure 2 suggests the specific nature of the two pockets on Parkin by lack of pUb/pNEDD8 interaction with the RING0 pocket, we wanted to understand the role of K211N mutation in Parkin activation. Also, as pNEDD8 activates Parkin stronger than pUb (Fig. 1A), we wondered whether pNEDD8 would rescue the effect of K211N mutation. Interestingly, although, unlike Parkin H302A, Parkin K211N does not show any defect in its interaction with pNEDD8 (Extended Data Figure 2), both Parkin K211N and Parkin H302A are 2-fold less active than native Parkin in the presence of pNEDD8 (Fig. 4A). This observation is consistent with pUb-mediated Parkin activation ([31] and Extended Data Fig. 3). In the control lanes without pNEDD8, we noticed the basal level ubiquitination activity of Parkin K211N was less than WT Parkin (Fig. 4A). Therefore, we decided to test the time-course ubiquitination assay on Parkin WT/K211N without any activator. Interestingly, we noticed that K211N mutation leads to approximately a 2-fold reduction in the basal level of Parkin activity that is independent of any activator (Fig. 4B). Overall, this data suggests that the loss of K211N Parkin activity is not due to its inability to bind with pUb/pNEDD8 but rather to some unknown reason that needs to be explored further.

Intricate mechanism of activator specificity on the RING0 and RING1

In contrast to the previous study [29,31], our data suggests that the two pockets (RING0 and RING1) on Parkin specifically recognize pUbl and pUb/pNEDD8, respectively. Although the sequence comparison in Fig. 2E suggested that key residues are conserved between Ubl, Ub, and NEDD8, differences at some key positions may help determine the specificity. For example, L8 in Ub/NEDD8 is N8 in Ubl, which may not allow the binding of pUbl in the RING1 pocket (Fig. 2E & [29]). Also, the difference between key residues mentioned in Fig. 2 helps the specificity between pUb and pNEDD8 for the RING1 pocket. However, the inability of pUb/pNEDD8 to bind the RING0 pocket remains elusive.

Interestingly, electrostatic charge surface analysis of Parkin, pUbl, pUb, and pNEDD8 revealed a distinct charge distribution on the ubiquitin-like proteins/domain and the two pockets of Parkin (Fig. 5A-E). pUbl (Fig. 5A) is quite negatively charged compared to pUb (Fig. 5B) or pNEDD8 (Fig. 5C). Furthermore, the surroundings of the basic patch (K161, R163, K211) on the RING0 pocket are made up of electropositive groups (R104/R455) (Fig. 5D). However, the negatively charged (E300) residue is positioned above the basic patch (K151, H302, R305) on the RING1 pocket of Parkin (Fig. 5E). Interestingly, D60 on Ubl is substituted with N60 and K60 on Ub and NEDD8 (Fig. 2E), respectively. An electronegative charge on the 60th position of Ubl would make it more favorable for the RING0 pocket (Fig 5A, 5D). Similarly, N60/K60 on Ub/NEDD8 would not be suitable for interaction with the positively charged residues around the basic patch on the RING0 pocket (Fig. 5B-D).

To validate the structural analysis, we tested Parkin activation using pUb or pUb N60D. Interestingly, compared to pUb, pUb N60D showed higher activation of Parkin (Fig. 5F, Extended Data Fig. 4), suggesting pUb N60D binding in the RING0 pocket, thus leading to a larger displacement of RING2 and stronger activation.

To confirm the binding of pUb N60D in the RING0 pocket, we performed the RING2 displacement assay. While pUb binding did not lead to REP-RING2 displacement and showed binding only in the RING1 pocket (Fig. 6A, Fig. 3), pUb N60D resulted in REP-RING2 displacement and binding in both pockets on Parkin, leading to higher shift on SEC (Fig. 6A). Furthermore, K211N mutation leads to loss of pUb N60D binding in RING0 pocket and thus did not displace REP-RING2 (Fig. 6B). However, the H302A mutation perturbed the binding of pUb N60D in the RING1 pocket while binding with the RING0 pocket and thus displacement of REP-RING2 remained intact (Fig. 6B). Overall, this data establishes the mechanism of specificity on the RING0 pocket of Parkin.

Crystal structure of K211N Parkin reveals RING2 locked with RING0

As our data clearly showed that the loss of Parkin K211N activity is not due to its inability to bind with pUb/pNEDD8, we wanted to understand the molecular mechanism of the loss of Parkin activity in K211N Parkin. To understand this, we crystallized and determined the structure of the R0RBR (K211N) and pNEDD8 complex. The structure of R0RBR (K211N) and pNEDD8 complex was determined at 1.8 Å (Extended Data Table 1). Similar to R0RBR and pNEDD8 structure, R0RBR K211N and pNEDD8 structure shows only one molecule of pNEDD8 bound in the RING1 pocket, and overall Parkin conformation remains the same (Extended Data Fig. 5). However, closer inspection revealed that due to the K211N mutation, the RING0 conformation is changed and pushed towards RING2 (Fig. 7A, Extended Data Fig. 5). N211 forms hydrogen bond with R163 and pulls R163 away from the K161 (Fig. 7A, B). The new conformation of R163 in K211N Parkin forces F209 away from its earlier position (Fig. 7A, B). In the new conformation, R163 forms hydrogen bonds with Q165, carbonyl of D219, and N211 (Fig. 7 B). Due to the above conformational changes, RING0 is pushed closer to the RING2 domain (Fig. 7A, B). The latter changes lead to the formation of new hydrogen bonds between K435 (RING2) and carbonyl of T177 (RING0), N428 (RING2) and S181 (RING0) (Fig. 7B). Also, in K211N Parkin structure K161 (RING0) forms salt bridge with the D460 (RING2). Furthermore, H433 (RING2) forms a hydrogen bond with W462 (RING2) in the K211N structure (Fig. 7B). Compared to K211N, in the native Parkin structures, distances between atoms (from RING0 and RING2) involved in the above interactions are significantly large and do not form hydrogen bonds/salt bridge (Fig. 7B). The new interactions between RING0 and RING2, in K211N Parkin, would not allow displacement of RING2 and exposure of C431, required for Parkin activation. Furthermore, unlike flexible conformation of RING2 in native Parkin with pNEDD8 (Fig. 2A), lower B-factor of the RING2 in K211N structure confirms that the RING2 flexibility is reduced upon K211N mutation (Fig. 7C). Overall, our data shows that K211N mutation leads to conformational changes on Parkin restricting RING2 displacement and thus results in loss of Parkin activity that is independent of pUb/pNEDD8 binding.

Discussion

Mutations in the gene expressing Parkin E3 ligase lead to a familial form of Parkinson's disease (PD). Due to its key role, Parkin is one of the significant targets from a therapeutic

perspective. In the last few years, several groups have extensively contributed to understanding the mechanism of Parkin activation [8–32]. Many Parkin structures have helped immensely toward understanding the Parkin activation mechanism [10,14,15,22–27,29-32]. Disease mutation K211N (on RING0) leading to loss of pUb-mediated Parkin activation [23,31] was an interesting phenomenon from a therapeutics perspective. Last year, a group suggested pUb binding in the RING0 pocket and proposed a new feedforward mechanism independent of pUbl [29,31]. Disease mutations leading to loss of binding with its substrates make the design of the Parkin activator to cure PD even more challenging. Also, lack of substrate specificity may lead to unwanted catastrophic events in cells.

Unlike previously suggested, we demonstrate that RING0 and RING1 pockets specifically bind with pUbl and pUb/pNEDD8, respectively. pUb and pNEDD8 can bind with RING1; however, pNEDD8 shows optimum binding and higher activation, suggesting a preference for pNEDD8 over pUb binding in the RING1 pocket (Fig. 1 & 2). Unlike previously proposed, pUb/pNEDD8 do not bind in the RING0 pocket (Fig 3 & Extended Data Fig. 2). RING0 pocket on Parkin is recognized explicitly by the pUbl domain of Parkin, which could be utilized to activate Parkin in trans as suggested by our recent work [30]. The higher affinity of the RING1 pocket for NEDD8 and Parkin activation with unphosphorylated NEDD8 (Fig. 1B) could be helpful in the context of previous findings, which showed overexpression of NEDD8 activation enzyme rescue the defects caused by silencing of PINK1 [33].

Several human Parkin and pUb complexes were crystallized by cross-linking of pUb-3Br with Q347C in the IBR domain of Parkin [22,23,26,30]. The fact that RING2 remains in the closed state in the pUb bound structures could be due to the tethering of pUb and thus restricting the domain movements on Parkin. Unlike the human Parkin and pUb complex, we determine the structure of pNEDD8 bound Parkin without any cross-linking. However, despite the more robust binding and higher activation of pNEDD8 than pUb (Fig. 1), RING2 was not displaced in the Parkin structure bound with pNEDD8 (Fig. 2). The crystal structure is also supported by the RING2 displacement assay, which confirms RING2 remains associated with the protein core after pUb/pNEDD8 binding (Fig 3 Extended Data Fig. 2). However, N60D mutation on ubiquitin that mimics the Ubl domain of Parkin results in binding on the RING0 pocket, resulting in RING2 displacement from the core of Parkin (Fig. 5 & 6). pUbl and pUb/pNEDD8 binding due to their specific binding on the two distinct pockets of Parkin leads to larger/faster and smaller/slower displacement of RING2, respectively.

While it was believed that disease mutation K211N in the RING0 pocket on Parkin leads to loss of binding with pUb [29,31], we demonstrate that K211N mutation does not affect Parkin interaction with pUb (Fig. 3). Furthermore, we discovered that K211N mutation leads to loss of Parkin activity independent of pUb/pNEDD8 binding (Fig. 4). The latter was further confirmed by Parkin K211N structure (Fig. 7). The structure of K211N shows conformational changes in the RING0 domain, which restricts the flexibility of RING2 by locking it with RING0 (Fig. 8) thus leading to loss of activity which is independent of pUb/pNEDD8 binding. The latter also explains a previous study showing K211N mutation reducing Parkin (lacking Ubl domain or Ser65) recruitment on mitochondria [31]. However, unlike previously believed, the defect in Parkin recruitment is not due to loss of pUb interaction with Parkin K211N. Rather, it is due to the conformational changes that lead to loss of Parkin activity, which would reduce the pUb levels (Fig. 8). The latter is further supported by our recent work, which shows that K211N Parkin (C431F), unlike H302A (C431F) Parkin, recruitment on mitochondria did not show any defect when it was co-expressed with native Parkin [30]. This discovery is relevant for designing small-molecule activators against Parkin by pharmaceutical companies. Additionally, it highlights the importance of a detailed structural analysis of various disease mutations on Parkin to help drug design against Parkinson's disease.

Authors' contributions

DRL performed all experiments, solved structures, and analyzed the data. SC purified various proteins. AK designed and supervised the research, refined structures, analyzed the data, and arranged funding. AK wrote the manuscript with input from DRL.

Acknowledgments

We thank Prof. Helen Walden and Prof. Miratul M. Muqit for useful discussions. We also thank Prof. Deepak Nair (RCB, Faridabad) and the Department of Biotechnology (Govt of India) for access to beamtime on ESRF. We thank the ESRF (ID30B), Grenoble, France, and support staff for data collection. The authors also acknowledge Shakti Dahe and other members of the AK group helping with various reagents. DRL is a PMRF fellow. AK is a recipient of the Innovative Young Biotechnology Award (DBT/12/IYBAl2019/03) and Ramalingaswami Fellowship (DBT/RLF/Re-entry/42/2019), which funded this project. AK also acknowledges IISER, Bhopal, and SERB (SERB/F/6520/2019-2020) for funding.

Conflict of interest

The authors declare no conflict of interest.

Figure legends

Figure 1. Parkin activation assay using NEDD8/Ub

A Ubiquitination assay to check Parkin activation with increasing concentrations of pUb or pNEDD8. The lower panel shows Miro1 ubiquitination. Coomassie-stained gels showing Parkin/Miro1 are used as the loading control. The ATP-independent band is indicated (*). The bar graph (left panel) shows the integrated intensities (mean ± s.e.m.) of ubiquitination levels from three independent experiments, as shown in the right panel. Statistical significance (***$P < 0.001$) was determined using a Pair-wise student's t-test.

B Ubiquitination assay to check Parkin activation with increasing concentrations of unphosphorylated Ub or NEDD8.

Figure 2. Crystal structure of Parkin with pNEDD8

A B-factor analysis on the crystal structure of Parkin (R0RBR) complex with pNEDD8. Scale is included to show the color-wise distribution of the B-factor, min (blue) to max (red).

B Overlay of pUb (grey) bound Parkin (light grey) (PDB: 5N2W) and pNEDD8 (cyan) bound Parkin (colored domain-wise) structures.

C Interactions between Parkin (light grey) and pUb (grey) (5N2W) in the basic patch of RING1. The distance between N60 of pUb and carbonyl of 187th amino acid of Parkin is highlighted.

D Interactions between Parkin (colored domain-wise) and pNEDD8 (cyan) in the basic patch of RING1. Unique hydrogen bonds between Parkin and pNEDD8 are highlighted with the dashed line.

E Sequence alignment of Ubl (Parkin), Ub, and NEDD8. Favorable residues on NEDD8 for its interaction in the RING1 pocket are marked with an arrow.

Figure 3. RING2 displacement assay to check pUb binding in the RING0 pocket

A SEC assay on Parkin (R0RBR, TEV treated) and pUB (with CBD-tag). A colored key is provided for each trace. Coomassie-stained gels of indicated fractions are shown.

B SEC assay on Parkin (R0RBR K211N, TEV treated) and pUB (with CBD-tag).

C SEC assay on (R0RBR H302A, TEV treated) and pUB (with CBD-tag).

The lower panel is a schematic representation to explain the SEC data from panels A, B, and C.

Figure 4. K211N mutation leads to loss of Parkin activity independent of pUb binding

A Ubiquitination assay to check WT/K211N/H302A Parkin activation with increasing concentrations of pNEDD8. The lower panel shows Miro1 ubiquitination. Coomassie-stained gels showing Parkin/Miro1 are used as the loading control. The ATP-independent band is indicated (*). The bar graph (left panel) shows the integrated intensities (mean ± s.e.m.) of ubiquitination levels from three independent experiments, as shown in the right panel. Statistical significance (***$P < 0.001$) was determined using a Pair-wise student's t-test.

B Time-course ubiquitination assay to compare the basal activity of WT Parkin or K211N Parkin in the absence of any activator (pUb/pNEDD8).

Figure 5. Unique charge distribution determining substrate specificity

A Electrostatic surface and charge distribution on phospho-Ubl (pUbl) domain of Parkin.

B Electrostatic surface and charge distribution on phospho-ubiquitin (pUb).

C Electrostatic surface and charge distribution on phospho-NEDD8 (pNEDD8) domain of Parkin.

D Electrostatic surface and charge distribution around the basic patch on the RING0 domain of Parkin.

E Electrostatic surface and charge distribution around the basic patch on the RING1 domain of Parkin.

F Ubiquitination assay to check Parkin activation with increasing concentrations of pUb or pUb (N60D). The bar graph shows the integrated intensities (mean ± s.e.m.) of ubiquitination levels from three independent experiments, as shown in the Extended Data Figure 4.

. Statistical significance (***$P < 0.001$) was determined using a Pair-wise student's t-test.

Figure 6. RING2 displacement assay to determine the role of N60D Ubiquitin mutation

A SEC assay on Parkin (R0RBR, TEV treated) and pUB/pUb N60D (with CBD-tag). A colored key is provided for each trace. The displaced REP-RING2 peak after binding of pUb N60D in the RING0 pocket is marked with an arrow. Coomassie-stained gels of indicated fractions are shown in the lower panel.

B SEC assay on Parkin (R0RBR, TEV treated)/Parkin (R0RBR K211N, TEV treated)/Parkin (R0RBR H302A, TEV treated) and pUb N60D (with CBD-tag). A colored key is provided for each trace.

The lower panel is a schematic representation to explain the SEC data from panels A and B.

Figure 7. Crystal structure of Parkin (R0RBR, K211N) and pNEDD8 reveal mechanism of loss of Parkin (K211N) activity

A Overlay of native Parkin (apo or bound with pUb/pNEDD8) structures and pNEDD8 bound with K211N Parkin structure. RING0 and RING2 domains from various native Parkin structures are shown in shades of grey. RING0 (orange) and RING2 (cyan) domains of K211N Parkin are shown. Conformational shifts in the RING0 domain of K211N Parkin are highlighted with the black arrow. Conformational shifts between RING0 and RING2 are highlighted with the red arrow (K211N Parkin) or green arrow (native Parkin), Cα of Q178 (RING0), and Cα of K435 (RING2) were used as reference points. RING0 pocket with repositioned side chains (stick) due to K211N is highlighted with an arrow.

B Standalone structures of K211N Parkin (upper panel) and native Parkin (lower panel) to highlight conformational changes. Hydrogen bonds are shown with a dashed line (upper panel), and the distance between the same atoms is highlighted with an arrow (lower panel). The salt bridge between K161 (RING0) and D460 (RING2) is highlighted (upper panel).

C B-factor analysis on the crystal structure of Parkin (R0RBR, K211N) with pNEDD8. Scale is included to show the color-wise distribution of the B-factor, min (blue) to max (red).

Figure 8. Model depicting mechanisms of pUb/pNEDD8-mediated Parkin activation, and K211N mutation leading to loss of Parkin activity

Extended Data Figure 1. Analysis of Parkin and pNEDD8 structure

A Superimposition of pNEDD8 (cyan) bound Parkin (R0RBR, different domains are colored) structure and pUB (grey) bound Parkin (grey) structure (5N2W).

B The 2Fo-Fc map (grey) of the R0RBR (colored as panel A) and pNEDD8 (cyan) structure. The 2Fo-Fc map is contoured at 1.2 σ.

C B-factor analysis on the crystal structure of R0RBR (4I1H). Scale is included to show the color-wise distribution of the B-factor, min (blue) to max (red).

Extended Data Figure 2. SEC assay to check RING2 displacement in the presence of pNEDD8

A SEC assay on Parkin (R0RBR, TEV treated) and pNEDD8 (with His-SUMO tag). A colored key is provided for each trace. Coomassie-stained gels of indicated fractions are shown in the lower panel.

B SEC assay on Parkin (R0RBR K211N, TEV treated) and pNEDD8 (with His-SUMO tag).

C SEC assay on Parkin (R0RBR H302A, TEV treated) and pNEDD8 (with His-SUMO tag).

Extended Data Figure 3. Ubiquitination assay on Parkin mutants in the presence of pUb

Ubiquitination assay to check WT/K211N/H302A Parkin activation with increasing concentrations of pUb. The lower panel shows Miro1 ubiquitination. Coomassie-stained gel showing Parkin/Miro1 is used as the loading control. The ATP-independent band is indicated (*).

Extended Data Figure 4. Ubiquitination assay on Parkin using pUb or pUb N60D

The representative assay used for quantification in Fig. 5 F.

Extended Data Figure 5. Analysis of Parkin K211N and pNEDD8 structure

Superimposition of various Parkin (both apo and in complex with pUb/pNEDD8) structures (different shades of grey) and pNEDD8 (green) bound R0RBR K211N (domains colored) structure.

Methods

Molecular cloning

Human Parkin and several other constructs used in this study were made as per the details provided in our recent manuscript [30]. Various Parkin mutations were generated using site-directed mutagenesis (SDM). A TEV protease site was introduced between 382nd -388th as explained in our recent manuscript [30]. NEDD8 gene was PCR amplified from cDNA from HEK393T cells and cloned in pET15b vector with His-SUMO tag. The Ub-Intein-CBD (Chitin Binding Domain) construct was made by cloning the ubiquitin gene (residues 1-75) in the pTXB-1 vector with His-tag (introduced after CBD using SDM). Pediculus humanus

corporis PINK1 (115 - 575) was a gift from David Komander [34](Addgene plasmid # 110750). Ube1 was a gift from Cynthia Wolberger [35](Addgene plasmid # 34965).

Protein expression and purification

Parkin constructs were expressed in *E. coli* BL21(DE3)pLysS cells. For Parkin (141-465) expression, the cells were grown till the OD reached 0.5-0.6, the temperature was brought down to 18°C, and induced with 50 µM IPTG in supplement with 400 µM $ZnCl_2$. The cells were pellet down and lysed by sonication in the lysis buffer (25 mM Tris pH 7.5, 300 mM NaCl, 5 mM Imidazole, and 100 µM AEBSF). The lysate was clarified using centrifugation at 35,000g for 1 hour. His-tagged proteins were trapped using Ni-NTA resin. Unbound proteins were washed using wash buffer (25 mM Tris pH 7.5, 350 mM NaCl, 10 mM Imidazole). His-tagged proteins were eluted using elution buffer (25 mM Tris pH 7.5, 300 mM NaCl, 250 mM Imidazole). His-SUMO was removed using SENP1 protease. All Parkin constructs were further purified over Anion exchange column Hi-trap Q HP (GE Healthcare) followed by Hiload 16/600 Superdex 200pg column (GE Healthcare) pre-equilibrated with storage buffer (25 mM Tris pH 7.5, 75 mM NaCl, 0.25 mM TCEP). SUMO-NEDD8 and Ubiquitin-CBD constructs were expressed the same as above without $ZnCl_2$. After elution from Ni-NTA, proteins were purified over Hiload 16/600 Superdex 200pg column (GE Healthcare) pre-equilibrated with storage buffer (25 mM Tris pH 7.5, 75 mM NaCl, 0.25 mM TCEP). GST-PhPINK1, NEDD8, Ubiquitin, Miro1, UbcH7, Ube1, and several other constructs used in this study were purified as above and as mentioned in our recent manuscript [30].

Ubiquitination Assay

Ubiquitination assays were carried out using full-length Parkin constructs. Reactions were performed at 25°C for 25 minutes in a buffer containing 25 mM Tris pH 7.5, 50 mM NaCl, 10 mM MgCl2, and 0.1 mM DTT, 5 mM ATP. All reactions contain 25 nM Ube1, 250 nM UbcH7 (E2), 1 µM of E3, and 2 µM of UbIR800. Ubiquitination on Miro1 was similar as above with 5 µM Miro1 and 0.5 µM Parkin at 25°C for 15 minutes. The ubiquitin labeling with IR800 dye was done using sulfo-Cyanine7.5 maleimide (Lumiprobe Life science solutions) as per the manufacturer's protocol [36], and UbIR800 was purified same as described in our recent work [30]. In Figure 1A, 1B, and Extended Data Figure 4A, reactions were carried out using increasing concentrations (1 µM, 2 µM, 4 µM) of pNEDD8/pUb/pUbN60D/Ub/NEDD8. Figure 4A and Extended Data Figure 3 used 1 µM and 2 µM of pNEDD8/pUb. Reactions were stopped by adding SDS dye and heating at 95°C for

5 mins. The samples were loaded on gradient gel and resolved using 1X MOPS running buffer. Gels were scanned using Li-COR® Odyssey Infrared Imaging System. All the reactions were repeated at least 3 times and quantified using ImageJ software [37]. For the quantification, ubiquitination on Miro1 was used in Figures 1A, 1B, 4A, and 5F. The first auto-ubiquitination event on Parkin was used for the quantification in Figure 4B. The statistical analysis was done using R.

Purification of phosphorylated proteins

GST-PhPINK1 was used for phosphorylation of Ubiquitin, Ubiquitin (N60D), and NEDD8 in buffer containing 50 mM Tris pH 8.5, 100 mM NaCl, 10 mM MgCl2, 10 mM DTT, and 10 mM ATP buffer at 25°C for 4 hrs. Completion of phosphorylation reaction was verified using Phos-Tag-Acrylamide (FUJIFILM). PhPINK1 was trapped using GSH resin, and flowthrough containing phosphorylated proteins were purified over Hiload 16/600 Superdex 75pg column (GE Healthcare) pre-equilibrated with buffer containing 25mM Tris pH 7.5, 75mM NaCl, 0.25mM TCEP.

Protein crystallization

Parkin R0RBR (141-465) or R0RBR K211N (141-465) were purified similarly as above up to ion exchange chromatography using Hitrap Q FF (GE Healthcare) column. Parkin was incubated with a 2-fold molar excess of phospho-NEDD8, and the complex was purified over Hiload 16/600 Superdex 75pg column (GE Healthcare) pre-equilibrated with buffer containing 25mM Tris pH 7.5, 75mM NaCl, 0.25mM TCEP. Crystals of the R0RBR complex were obtained in 0.2 M Sodium sulfate, 0.1 M Bis-Tris propane 7.5, 20 % w/v PEG 3350 at 4°C. Crystals of the R0RBR K211N complex were obtained in 0.1M MMT 8.0, 25 % w/v PEG 1500 at 18°C. R0RBR and R0RBR K211N crystals with pNEDD8 were vitrified using their mother liquor containing 20% ethylene glycol and 20% PEG 400, respectively.

Data collection and Structure determination

Data was collected at ID30B of the European Synchrotron Radiation Facility (ESRF), Grenoble, France. Data were processed using XDS [38] and Xia2 [39] for R0RBR and R0RBR K211N, respectively. Aimless in CCP4 suite [40] was used for data scaling. Structures were determined using Phaser [41]. R0RBR (PDB id: 4I1H) and NEDD8 (PDB id: 1NDD) were used

as search models. The models were built in Coot [42] and refined in Refmac5 [43]. Data were deposited in the protein data bank, and PDB codes are included in Extended Data Table 1.

Size-exclusion chromatography assay

All the binding experiments were performed using the Superdex 75increase 10/300 GL column (GE Healthcare). 500 µl of reaction volume containing 20 µM Phospho-Ub (CBD tag)/phospho-UbN60D (CBD tag)/phospho-NEDD8 (His-SUMO tag) were incubated with 10 µM of R0RBR (TEV treated and TEV depleted)/ R0RBR K211N (TEV treated and TEV depleted)/ R0RBR H302A (TEV treated and TEV depleted) 30minutes on ice before injection. Fractions of each run were analyzed by SDS-PAGE.

References

1. Bonifati, V. *et al*. Autosomal recessive early onset parkinsonism is linked to three loci: PARK2, PARK6, and PARK7. *Neurol. Sci.* **23 Suppl 2**, (2002).
2. Martin, I., Dawson, V. L. & Dawson, T. M. Recent Advances in the Genetics of Parkinson's Disease. *Annu. Rev. Genomics Hum. Genet.* **12**, 301 (2011).
3. Kitada, T. *et al.* Mutations in the parkin gene cause autosomal recessive juvenile parkinsonism. *Nature* **392**, 605–608 (1998).
4. Valente, E. M. *et al*. Hereditary early-onset Parkinson's disease caused by mutations in PINK1. *Science* **304**, 1158–1160 (2004).
5. Chung, S. Y. *et al.* Parkin and PINK1 Patient iPSC-Derived Midbrain Dopamine Neurons Exhibit Mitochondrial Dysfunction and α-Synuclein Accumulation. *Stem Cell Reports* **7**, 664 (2016).
6. Exner, N., Lutz, A. K., Haass, C. & Winklhofer, K. F. Mitochondrial dysfunction in Parkinson's disease: molecular mechanisms and pathophysiological consequences. *EMBO J.* **31**, 3038–3062 (2012).
7. Narendra, D., Walker, J. E. & Youle, R. Mitochondrial quality control mediated by PINK1 and Parkin: links to parkinsonism. *Cold Spring Harb. Perspect. Biol.* **4**, (2012).
8. Chaugule, V. K. *et al*. Autoregulation of Parkin activity through its ubiquitin-like domain. *EMBO J.* **30**, 2853–2867 (2011).

9. Spratt, D. E., Walden, H. & Shaw, G. S. RBR E3 ubiquitin ligases: new structures, new insights, new questions. *Biochem. J.* **458**, 421–437 (2014).
10. Riley, B. E. *et al.* Structure and function of Parkin E3 ubiquitin ligase reveals aspects of RING and HECT ligases. *Nat. Commun. 2013 41* **4**, 1–9 (2013).
11. Wenzel, D. M., Lissounov, A., Brzovic, P. S. & Klevit, R. E. UBCH7 reactivity profile reveals parkin and HHARI to be RING/HECT hybrids. *Nature* **474**, 105–108 (2011).
12. Walden, H. & Rittinger, K. RBR ligase-mediated ubiquitin transfer: a tale with many twists and turns. *Nat. Struct. Mol. Biol.* **25**, 440–445 (2018).
13. Lechtenberg, B. C. *et al.* Structure of a HOIP/E2~ubiquitin complex reveals RBR E3 ligase mechanism and regulation. **529**, 546–550 (2016).
14. Trempe, J. F. *et al.* Structure of parkin reveals mechanisms for ubiquitin ligase activation. *Science* **340**, 1451–1455 (2013).
15. Wauer, T. & Komander, D. Structure of the human Parkin ligase domain in an autoinhibited state. *EMBO J.* **32**, 2099–2112 (2013).
16. Kane, L. A. *et al.* PINK1 phosphorylates ubiquitin to activate Parkin E3 ubiquitin ligase activity. *J. Cell Biol.* **205**, 143–153 (2014).
17. Kazlauskaite, A. *et al.* Parkin is activated by PINK1-dependent phosphorylation of ubiquitin at Ser65. *Biochem. J.* **460**, 127 (2014).
18. Koyano, F. *et al.* Ubiquitin is phosphorylated by PINK1 to activate parkin. *Nature* **510**, 162–166 (2014).
19. Kazlauskaite, A. *et al.* Binding to serine 65-phosphorylated ubiquitin primes Parkin for optimal PINK1-dependent phosphorylation and activation. *EMBO Rep.* **16**, 939 (2015).
20. Kondapalli, C. *et al.* PINK1 is activated by mitochondrial membrane potential depolarization and stimulates Parkin E3 ligase activity by phosphorylating Serine 65. *Open Biol.* **2**, (2012).
21. Shiba-Fukushima, K. *et al.* PINK1-mediated phosphorylation of the Parkin ubiquitin-like domain primes mitochondrial translocation of Parkin and regulates mitophagy. *Sci. Rep.* **2**, (2012).
22. Gladkova, C., Maslen, S. L., Skehel, J. M. & Komander, D. Mechanism of parkin activation by PINK1. *Nature* **559**, 410–414 (2018).
23. Wauer, T., Simicek, M., Schubert, A. & Komander, D. Mechanism of phospho-ubiquitin induced PARKIN activation. *Nature* **524**, 370 (2015).
24. Kumar, A. *et al.* Disruption of the autoinhibited state primes the E3 ligase parkin for

activation and catalysis. *EMBO J.* **34**, 2506–2521 (2015).

25. Sauvé, V. *et al.* A Ubl/ubiquitin switch in the activation of Parkin. *EMBO J.* **34**, (2015).
26. Kumar, A. *et al.* Parkin–phosphoubiquitin complex reveals cryptic ubiquitin-binding site required for RBR ligase activity. *Nat. Struct. Mol. Biol. 2017 245* **24**, 475–483 (2017).
27. Sauvé, V. *et al.* Mechanism of parkin activation by phosphorylation. *Nat. Struct. Mol. Biol.* **25**, 623–630 (2018).
28. Stuber, K. *et al.* Structural and functional consequences of NEDD8 phosphorylation. *Nat. Commun. 2021 121* **12**, 1–15 (2021).
29. Fakih, R., Sauvé, V. & Gehring, K. Structure of the second phosphoubiquitin–binding site in parkin. *J. Biol. Chem.* **298**, 1 (2022).
30. Lenka, D. *et al.* Mechanism of feedforward Parkin activation by self-association. (2023) doi:10.21203/rs.3.rs-2859540/v2.
31. Sauvé, V. *et al.* Structural basis for feedforward control in the PINK1/Parkin pathway. *EMBO J.* **41**, e109460 (2022).
32. Condos, T. E. *et al.* Synergistic recruitment of UbcH7~Ub and phosphorylated Ubl domain triggers parkin activation. *EMBO J.* **37**, (2018).
33. Choo, Y. S. *et al.* Regulation of parkin and PINK1 by neddylation. *Hum. Mol. Genet.* **21**, 2514–2523 (2012).
34. Schubert, A. F. *et al.* Structure of PINK1 in complex with its substrate ubiquitin. **552**, 51–56 (2017).
35. Berndsen, C. E. & Wolberger, C. A spectrophotometric assay for conjugation of ubiquitin and ubiquitin-like proteins. *Anal. Biochem.* **418**, 102–110 (2011).
36. Sabuncu, S. *et al.* Protein-Coated Biodegradable Gas-Stabilizing Nanoparticles for Cancer Therapy and Diagnosis Using Focused Ultrasound. *Adv. Mater. Interfaces* **10**, (2023).
37. Schindelin, J. *et al.* Fiji: an open-source platform for biological-image analysis. *Nat. Methods 2012 97* **9**, 676–682 (2012).
38. Kabsch, W. XDS. *Acta Crystallogr. Sect. D Biol. Crystallogr.* **66**, 125 (2010).
39. Gildea, R. J. *et al.* Xia2.multiplex: A multi-crystal data-Analysis pipeline. *Acta Crystallogr. Sect. D Struct. Biol.* **78**, 752–769 (2022).
40. The CCP4 suite: programs for protein crystallography. *Acta Crystallogr. D. Biol. Crystallogr.* **50**, 760–763 (1994).
41. McCoy, A. J. *et al.* Phaser crystallographic software. *urn:issn:0021-8898* **40**, 658–674

(2007).

42. Emsley, P. & Cowtan, K. Coot: model-building tools for molecular graphics. *Acta Crystallogr. D. Biol. Crystallogr.* **60**, 2126–2132 (2004).

43. Murshudov, G. N. *et al.* REFMAC5 for the refinement of macromolecular crystal structures. *urn:issn:0907-4449* **67**, 355–367 (2011).

Extended Data Table 1
Data collection and Refinement statistics

	Parkin and pNEDD8	Parkin K211N and pNEDD8
Data collection		
Resolution range	40.91 - 2.25 (2.331 - 2.25)	39.83 - 1.8 (1.864 - 1.8)
Space group	I 1 2 1	P 21 21 21
a, *b*, *c* (Å)	77.976, 47.747, 127.859	58.249, 74.603, 80.067
α, *β*, *γ* (°)	90, 105.38, 90	90, 90, 90
Total reflections	93740 (9602)	146049 (15003)
Unique reflections	21812 (2149)	32755 (3236)
Multiplicity	4.3 (4.5)	4.5 (4.6)
Completeness (%)	99.67 (99.95)	99.17 (99.32)
I/σ(I)	9.23 (1.76)	10.25 (2.98)
Wilson B-factor	35.54	17.67
R-merge	0.1159 (0.84)	0.09746 (0.4231)
CC1/2	0.993 (0.619)	0.996 (0.826)
Refinement		
Reflections used in refinement	21766 (2149)	32750 (3236)
R-work/R-free	0.2116/ 0.2509	0.1712/ 0.2090
No of Atoms		
macromolecules	2929	3045
ligands	20	29
solvent	174	324
RMS deviations		
Bond length (Å)	0.008	0.011
Bond angles (°)	1.25	1.76
Ramachandran favored (%)	95.64	96.55
Ramachandran outliers (%)	0	0.53
B-factors		

macromolecules	45.86	22.19
ligands	47.2	39.68
solvent	45.05	32.07
Accession code	8WZO	8WZN

Statistics for the highest-resolution shell are shown in parentheses

A

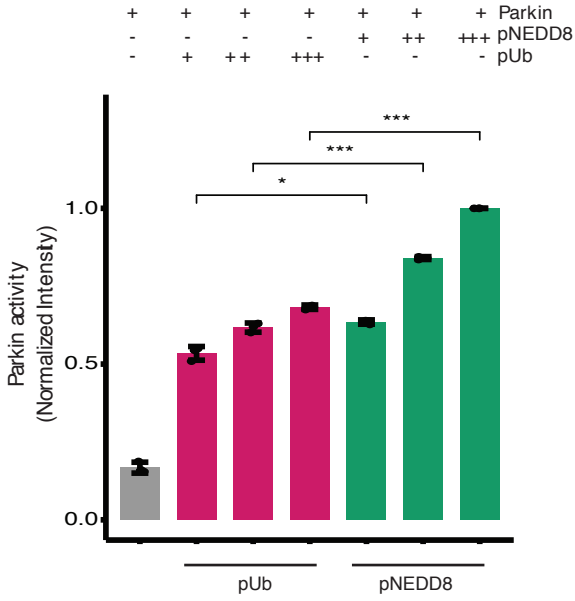
+ + + + + + + Parkin
- - - - + ++ +++ pNEDD8
- + ++ +++ - - - pUb
***
***
*
1.0
0.5
0.0
Parkin activity
(Normalized Intensity)
pUb
pNEDD8

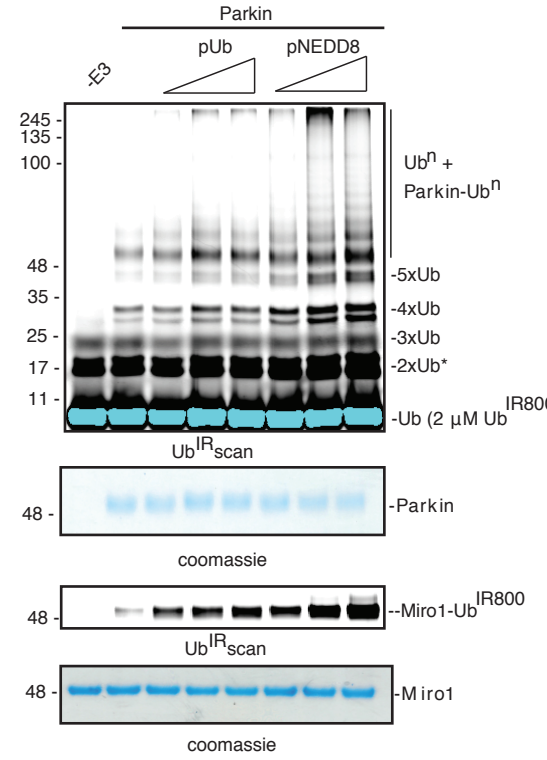
Parkin
pUb
pNEDD8
-E3
245
135
100
48
35
25
17
11
Ub^n +
Parkin-Ub^n
-5xUb
-4xUb
-3xUb
-2xUb*
-Ub (2 µM Ub^IR800)
Ub^IR scan
48
-Parkin
coomassie
48
--Miro1-Ub^IR800
Ub^IR scan
48
-Miro1
coomassie

B

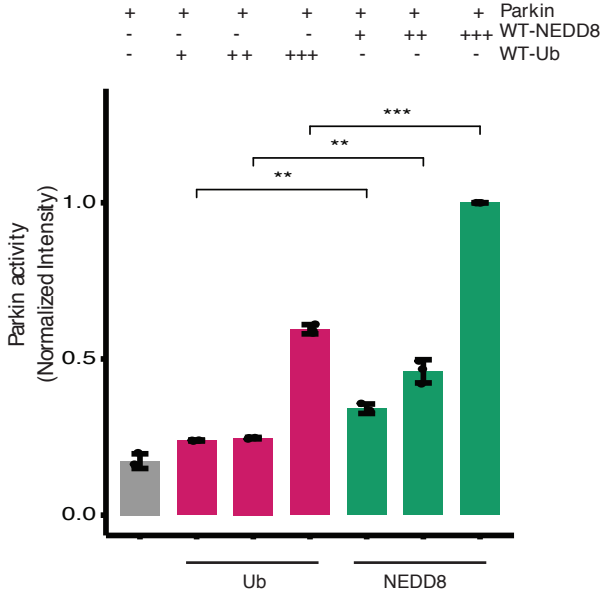
+ + + + + + + Parkin
- - - - + ++ +++ WT-NEDD8
- + ++ +++ - - - WT-Ub
***
**
**
1.0
0.5
0.0
Parkin activity
(Normalized Intensity)
Ub
NEDD8

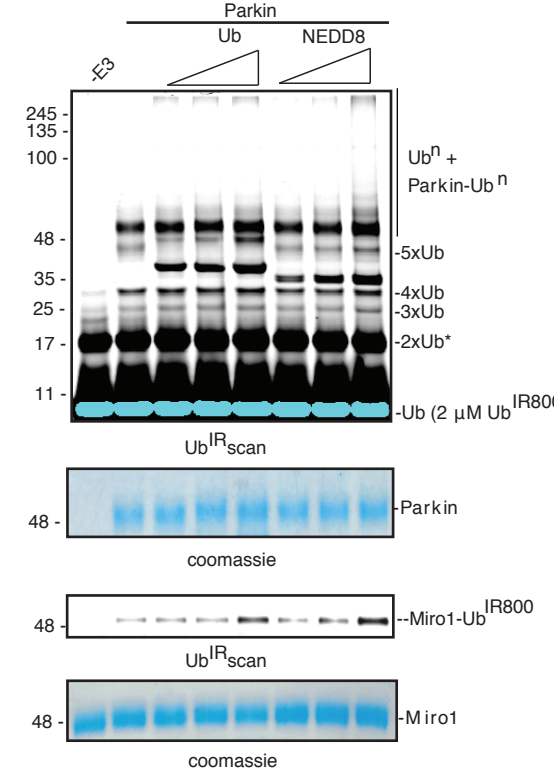
Parkin
Ub
NEDD8
-E3
245
135
100
48
35
25
17
11
Ub^n +
Parkin-Ub^n
-5xUb
-4xUb
-3xUb
-2xUb*
-Ub (2 µM Ub^IR800)
Ub^IR scan
48
-Parkin
coomassie
48
--Miro1-Ub^IR800
Ub^IR scan
48
-Miro1
coomassie

Figure 1

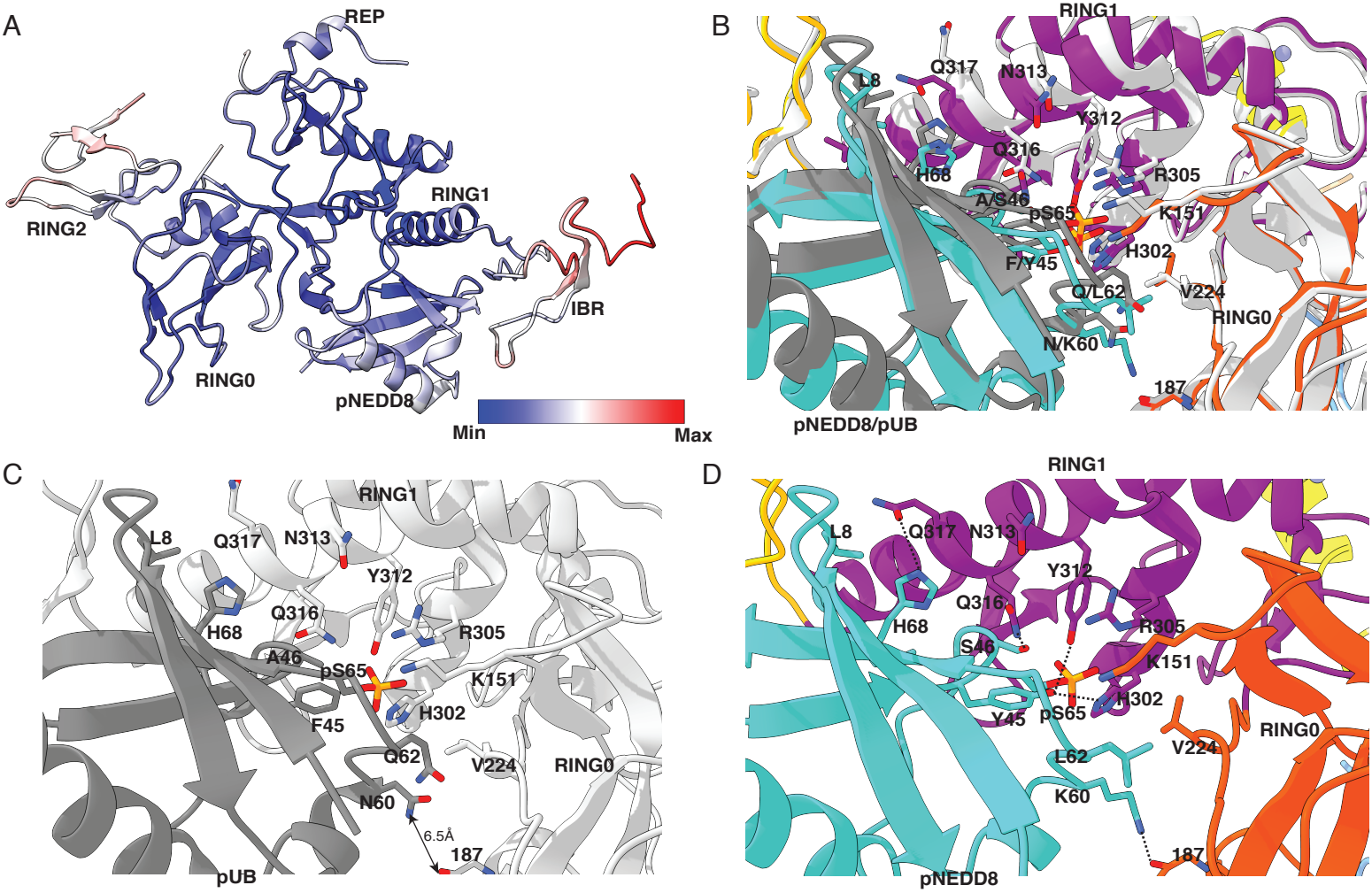
A
REP
RING2
RING1
IBR
RING0
pNEDD8
Min
Max
B
RING1
L8
Q317
N313
Y312
Q316
H68
R305
A/S46
pS65
K151
H302
F/Y45
Q/L62
V224
RING0
N/K60
187
pNEDD8/pUB
C
RING1
L8
Q317
N313
Y312
Q316
H68
R305
A46
pS65
K151
H302
F45
Q62
V224
RING0
N60
6.5Å
187
pUB
D
RING1
L8
Q317
N313
Y312
Q316
H68
R305
S46
K151
H302
Y45
pS65
RING0
V224
L62
K60
187
pNEDD8
E
1 10 20 30 40 50 60 70
Ubl(Parkin) MIVFVRFNSSHGFPVEVDSDTSIFQLKEVVAKRQGVPADQLRVIFAGKELRNDWTVQNCDLDQQSIVHIVQRPWRK
Ubiquitin MQIFVKTLTGKTITLEVEPSDTIENVKAKIQDKEGIPPDQQRLIFAGKQLEDGRTLSDYNIQKESTLHLVLRLRGG
NEDD8 MLIKVKTLTGKEIEIDIEPTDKVERIKERVEEKEGIPPQQQRLIYSGKQMNDEKTAADYKILGGSVLHLVLALRGG

Figure 2

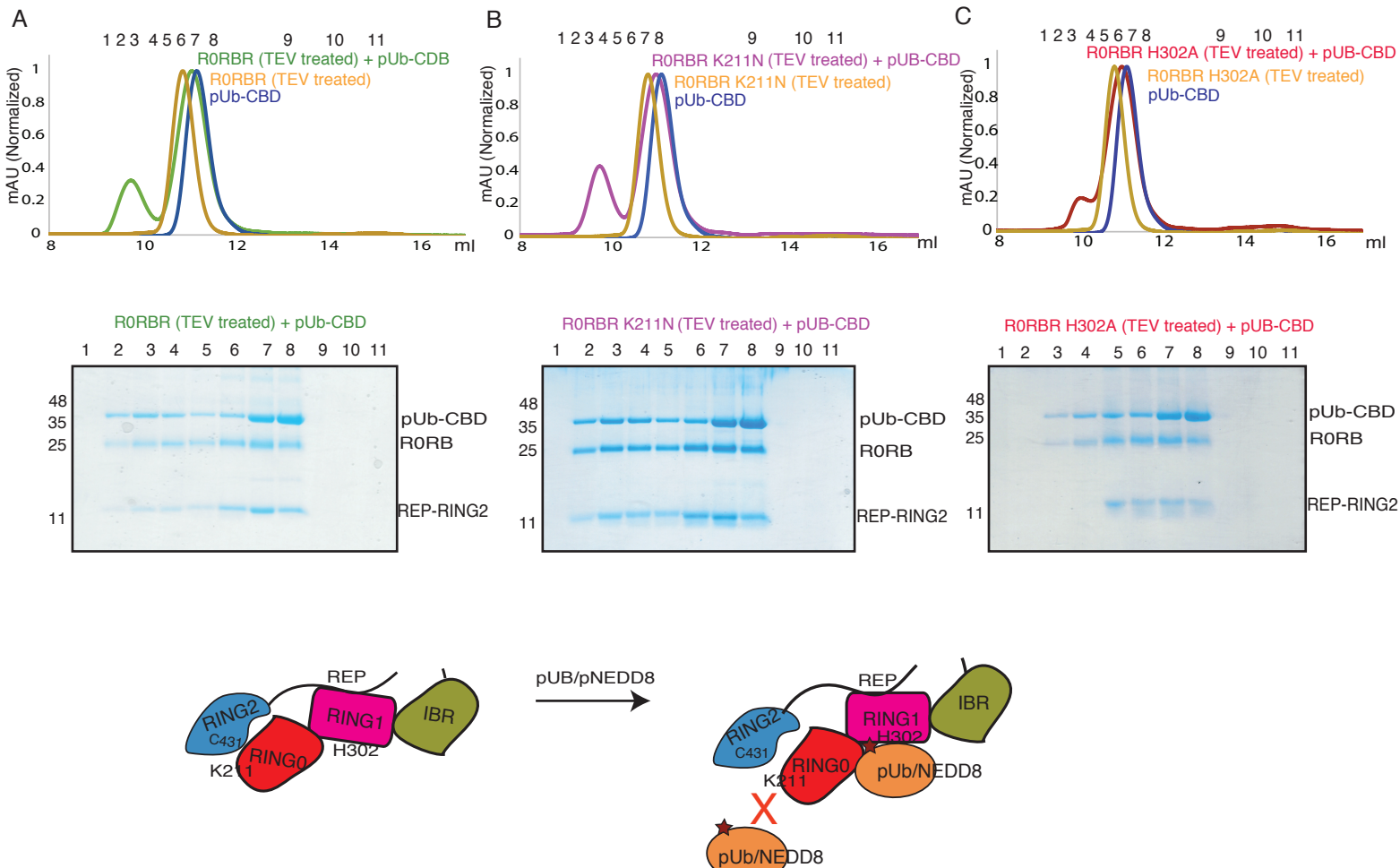
A
1 2 3 4 5 6 7 8 9 10 11
R0RBR (TEV treated) + pUb-CDB
R0RBR (TEV treated)
pUb-CBD
mAU (Normalized)
ml
B
R0RBR K211N (TEV treated) + pUB-CBD
R0RBR K211N (TEV treated)
pUb-CBD
C
R0RBR H302A (TEV treated) + pUB-CBD
R0RBR H302A (TEV treated)
pUb-CBD
R0RBR (TEV treated) + pUb-CBD
R0RBR K211N (TEV treated) + pUB-CBD
R0RBR H302A (TEV treated) + pUB-CBD
48
35
25
11
pUb-CBD
R0RB
REP-RING2
REP
RING2
C431
RING1
H302
IBR
RING0
K211
pUB/pNEDD8
pUb/NEDD8

Figure 3

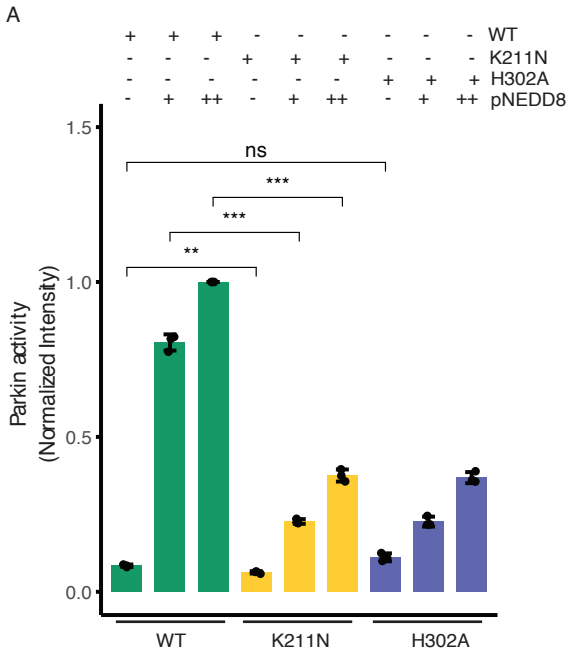
A
WT
K211N
H302A
pNEDD8
Parkin activity
(Normalized Intensity)
ns
***
***
**
WT
K211N
H302A

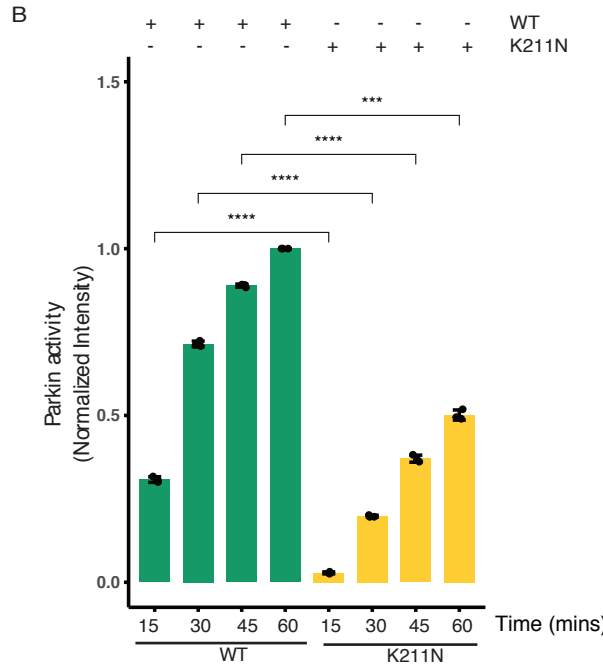
B
WT
K211N
Parkin activity
(Normalized Intensity)
***
****
****
****
Time (mins)
WT
K211N

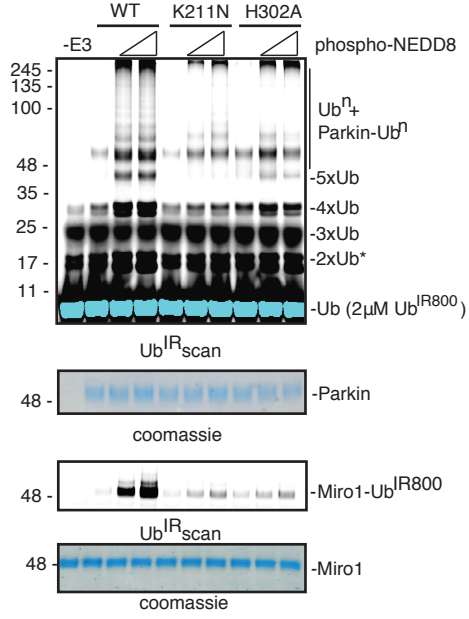
WT
K211N
H302A
-E3
phospho-NEDD8
Ub^n+
Parkin-Ub^n
-5xUb
-4xUb
-3xUb
-2xUb*
-Ub (2µM Ub^IR800)
Ub^IR scan
-Parkin
coomassie
-Miro1-Ub^IR800
Ub^IR scan
-Miro1
coomassie

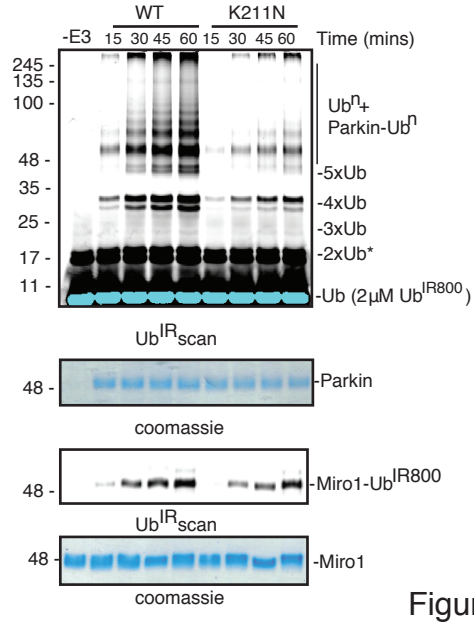
WT
K211N
-E3
Time (mins)
Ub^n+
Parkin-Ub^n
-5xUb
-4xUb
-3xUb
-2xUb*
-Ub (2µM Ub^IR800)
Ub^IR scan
-Parkin
coomassie
-Miro1-Ub^IR800
Ub^IR scan
-Miro1
coomassie

Figure 4

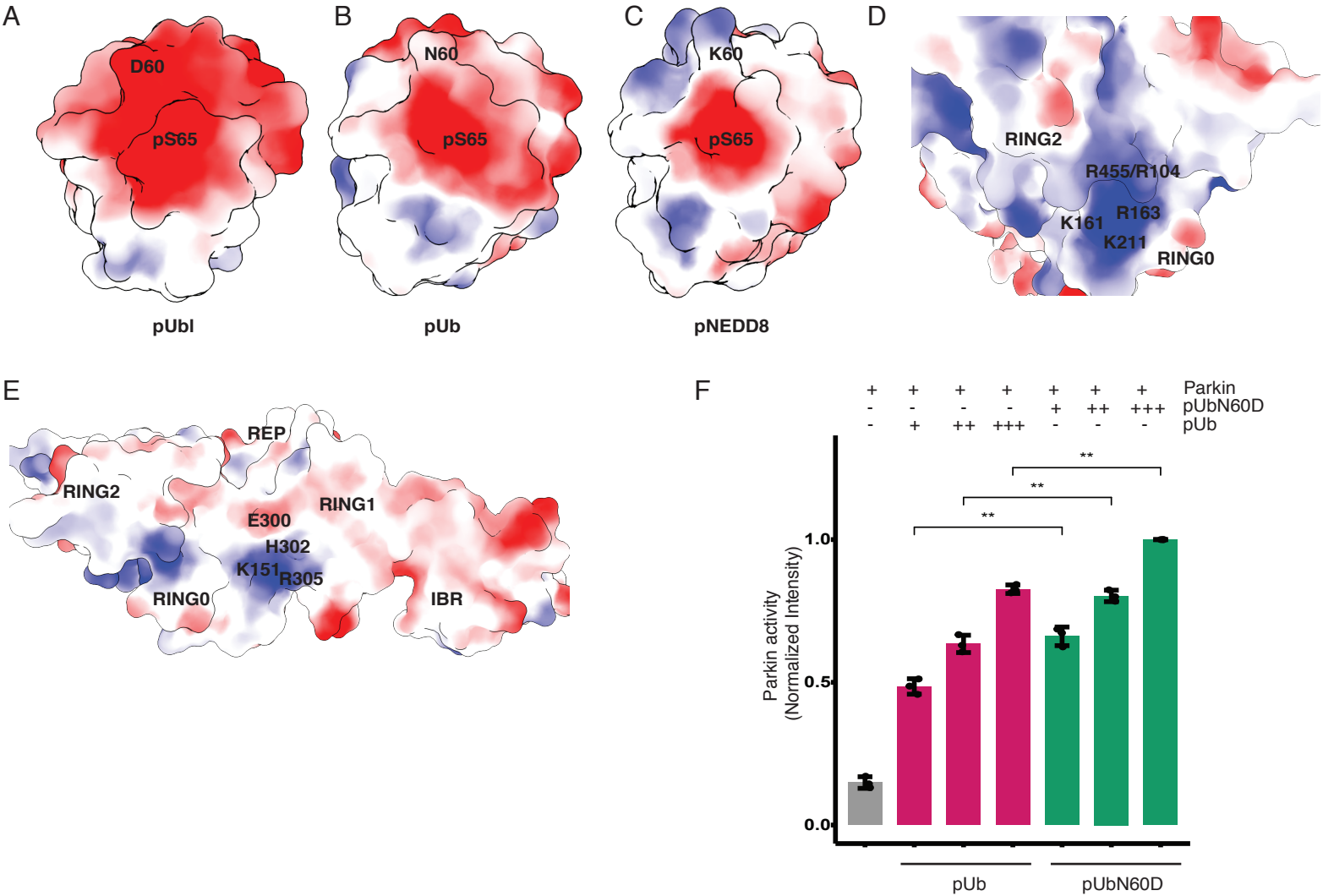
A
D60
pS65
pUbl
B
N60
pS65
pUb
C
K60
pS65
pNEDD8
D
RING2
R455/R104
R163
K161
K211
RING0
E
REP
RING2
RING1
E300
H302
K151
R305
RING0
IBR
F
Parkin
pUbN60D
pUb
Parkin activity
(Normalized Intensity)
1.0
0.5
0.0
**
pUb
pUbN60D

Figure 5

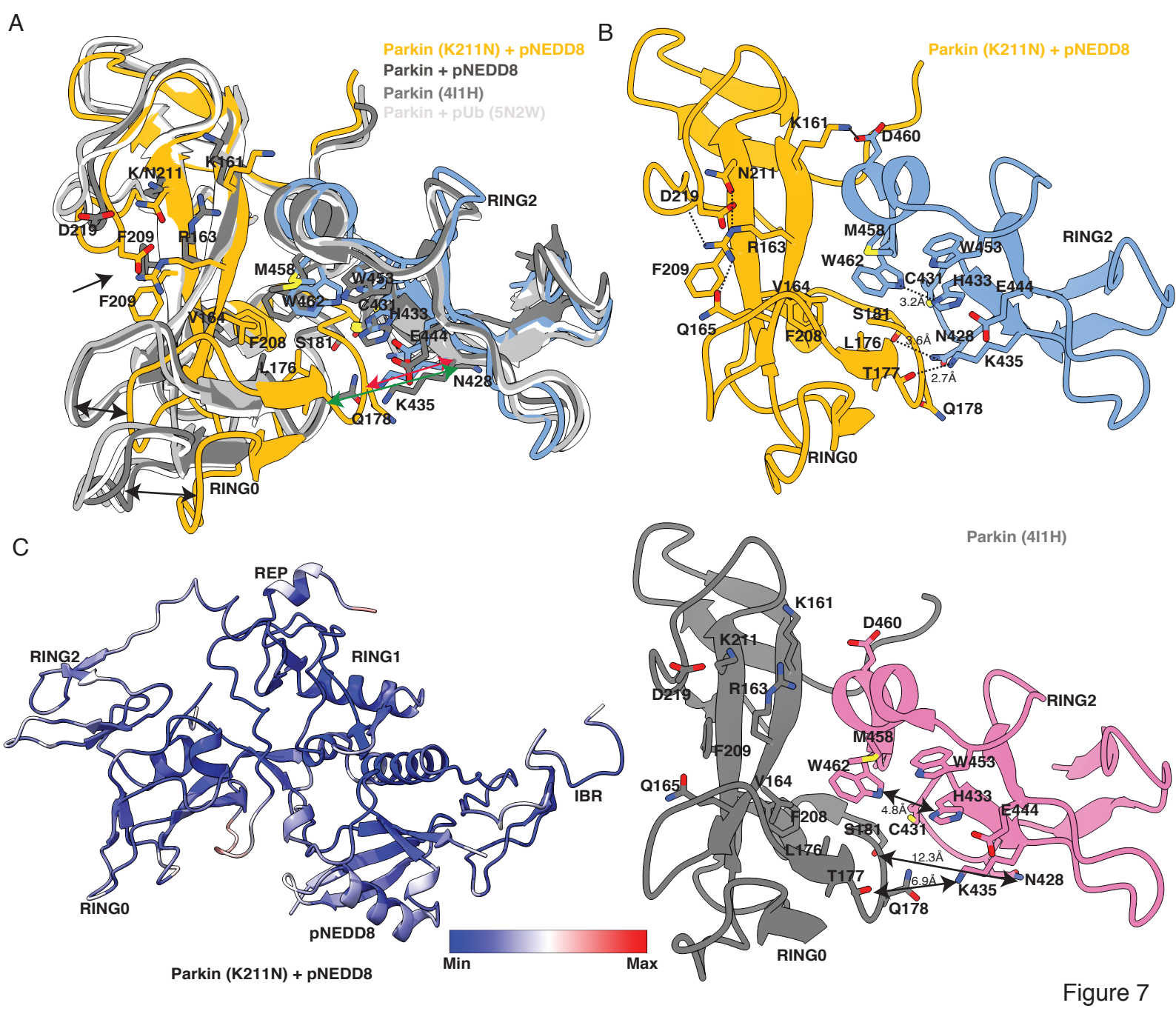
A
Parkin (K211N) + pNEDD8
Parkin + pNEDD8
Parkin (4I1H)
Parkin + pUb (5N2W)
K/N211
K161
D219
F209
R163
M458
W462
W453
C431
H433
E444
V164
F208
S181
L176
N428
K435
Q178
RING2
RING0
B
Parkin (K211N) + pNEDD8
K161
D460
N211
D219
R163
M458
W462
W453
RING2
F209
V164
C431
H433
E444
3.2Å
S181
Q165
F208
L176
3.6Å
N428
K435
T177
2.7Å
Q178
RING0
C
REP
RING2
RING1
IBR
RING0
pNEDD8
Min
Max
Parkin (K211N) + pNEDD8
Parkin (4I1H)
K161
D460
K211
D219
R163
RING2
M458
F209
W462
W453
Q165
V164
H433
4.8Å
E444
F208
S181
C431
L176
12.3Å
T177
6.9Å
K435
N428
Q178
RING0

Figure 7

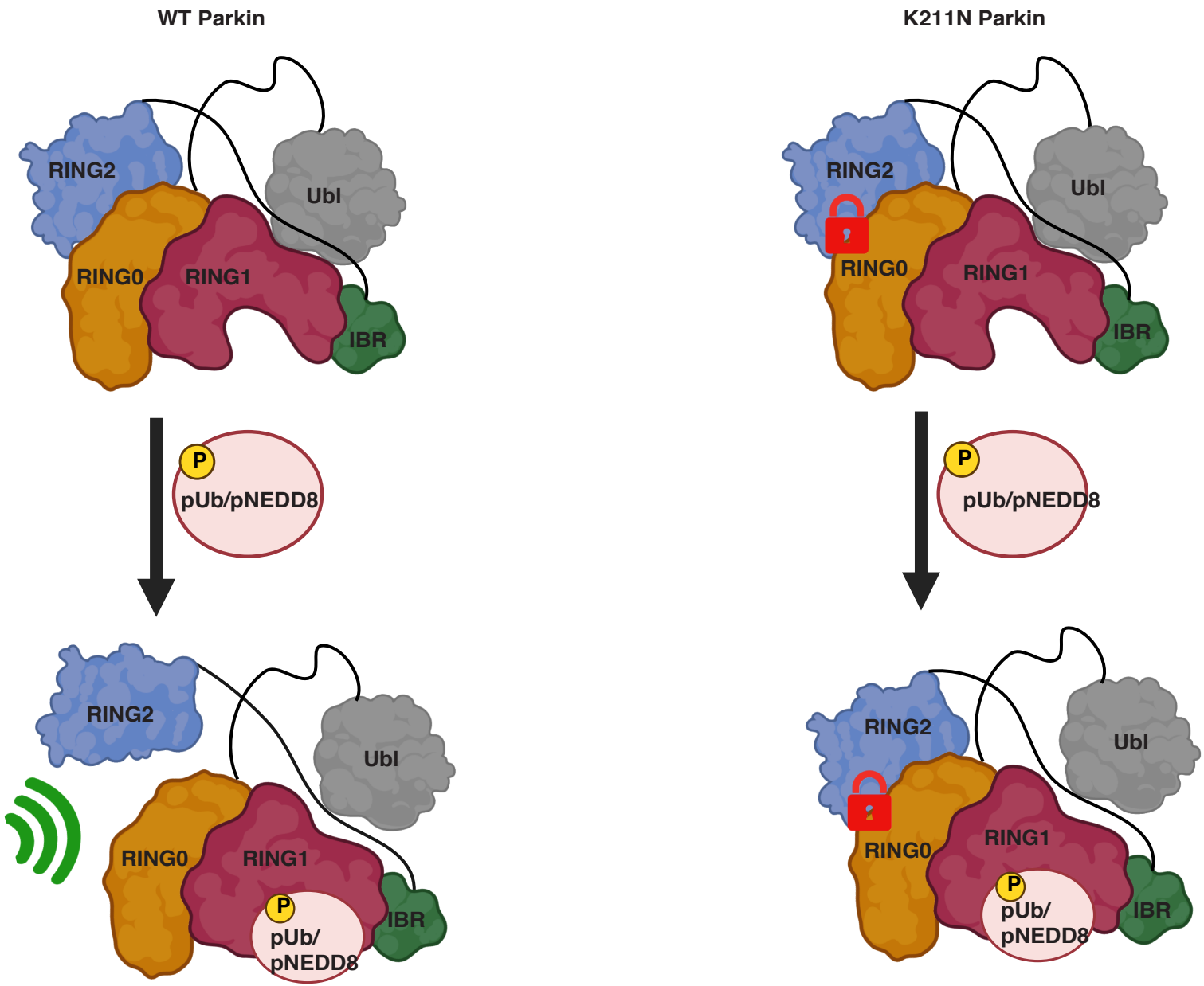
WT Parkin
RING2
Ubl
RING0
RING1
IBR
P
pUb/pNEDD8
RING2
Ubl
RING0
RING1
P
pUb/
pNEDD8
IBR
K211N Parkin
RING2
Ubl
RING0
RING1
IBR
P
pUb/pNEDD8
RING2
Ubl
RING0
RING1
P
pUb/
pNEDD8
IBR

Figure 8

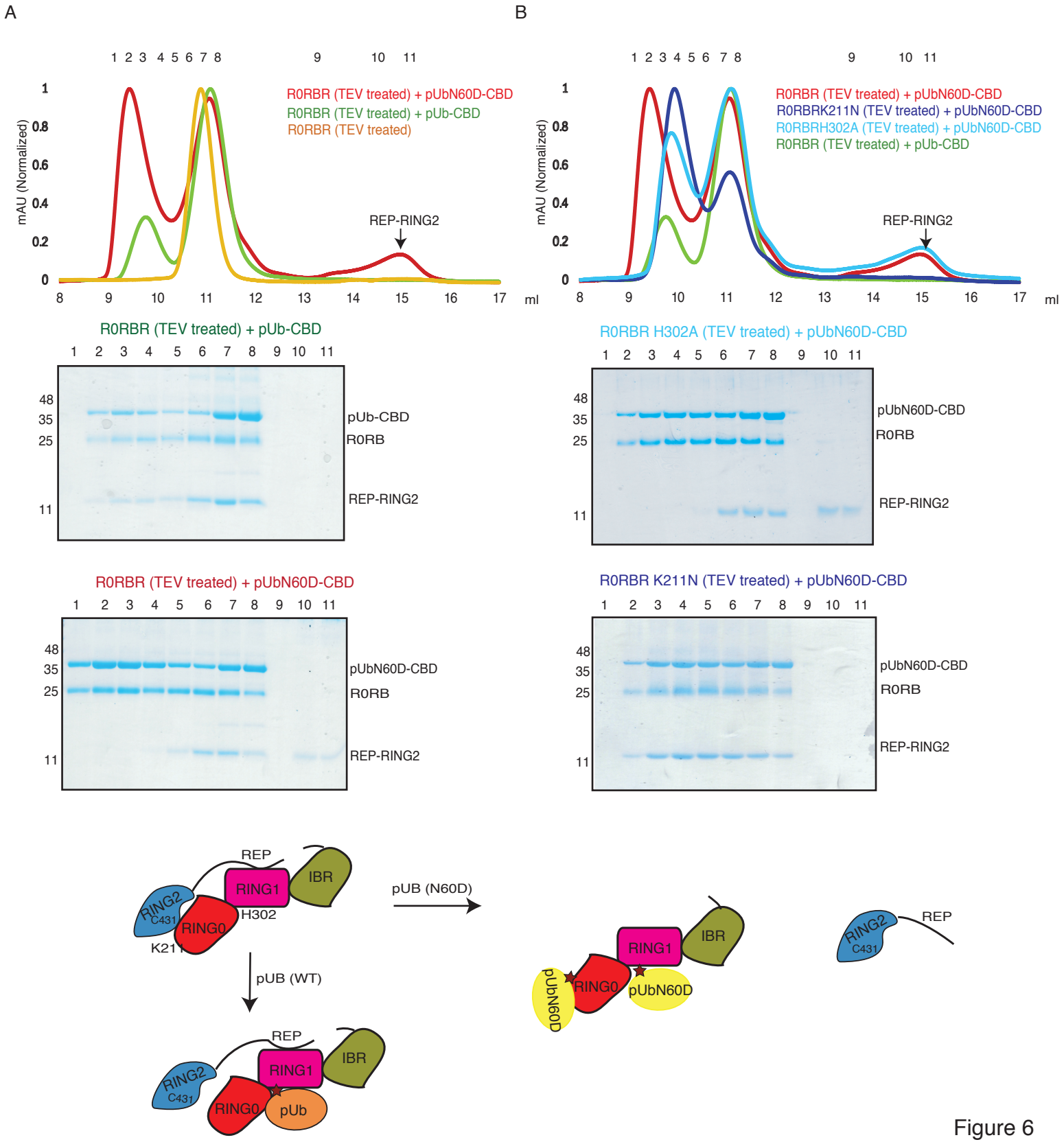
A
B
1 2 3 4 5 6 7 8 9 10 11
mAU (Normalized)
R0RBR (TEV treated) + pUbN60D-CBD
R0RBR (TEV treated) + pUb-CBD
R0RBR (TEV treated)
REP-RING2
ml
R0RBRK211N (TEV treated) + pUbN60D-CBD
R0RBRH302A (TEV treated) + pUbN60D-CBD
R0RBR (TEV treated) + pUb-CBD
R0RBR (TEV treated) + pUb-CBD
R0RBR H302A (TEV treated) + pUbN60D-CBD
R0RBR (TEV treated) + pUbN60D-CBD
R0RBR K211N (TEV treated) + pUbN60D-CBD
pUb-CBD
R0RB
REP-RING2
pUbN60D-CBD
REP
RING2
C431
RING1
IBR
RING0
H302
K211
pUB (N60D)
pUB (WT)
pUb
pUbN60D

Figure 6